Eur. Phys. J. B **39**, 149–154 (2004)
DOI: 10.1140/epjb/e2004-00191-0

THE EUROPEAN PHYSICAL JOURNAL B

Epitaxial growth of solution deposited $Bi_2Sr_2CaCu_2O_x$ films

O.F. Göbel[1], X. Du[1,a], T. Hibma[1], I. von Lampe[2], and U. Steiner[1,b]

[1] Materials Science Center, University of Groningen, Nijenborgh 4, 9747 AG Groningen, The Netherlands
[2] Institut für Werkstoffwissenschaften und -technologien, Technische Universität Berlin, Englische Straße 20, 10587 Berlin, Germany

Received 13 January 2004
Published online 29 June 2004 –

Abstract. The epitaxial growth of $Bi_2Sr_2CaCu_2O_x$ (Bi2212) high temperature superconducting thin films was studied. The films were solution-deposited from a polymer-containing precursor onto $SrTiO_3$ (001) substrates. Bi2212 formed an epitaxial phase with the **c**-axis parallel to the substrate normal and an in-plane orientation with the **a**-axis parallel to the $SrTiO_3$ [110] and [$\bar{1}$10] directions. This phase was found to be robust with respect to small changes in stoichiometry, where the appearance of an additional BiSrCuO phase was observed. This minority phase had no major effect on the epitaxial alignment of the Bi2212 phase or the critical temperature of the thin-film sample.

PACS. 81.15.-z Methods of deposition of films and coatings; film growth and epitaxy – 81.20.Fw Sol-gel processing, precipitation – 74.72.-h Cuprate superconductors (high-T_c and insulating parent compounds)

1 Introduction

Since the discovery of high temperature superconducting ceramic materials, there has been an increasing interest in the manipulation of these materials to fabricate thin films and wires. The applicability of high-T_c superconductors in thin films is, however, dependent on the epitaxial growth of the superconducting phase on a suitable substrate. Techniques for the production of high quality films include laser ablation [1,2], electron-beam evaporation [3], or chemical vapor deposition [4, 5]. While well established, these methods are typically slow, expensive, and not easily combinable with standard lithographic techniques. In an alternative process, high-T_c ceramic thin films can be made by a chemical solution deposition process. This technique employs a precursor solution of the constituent metal ions, which is solidified during the film manufacture process. Thin films of the high-T_c ceramic $YBa_2Cu_3O_x$ (Y123) were grown from precursor solutions of the corresponding metal acetates using 1,3-bis(dimethylamino)-2-propanol and acetic acid [6], from acetates and acetic acid [7], and from alkoxides, isopropanol, and acetic acid [8]. $YbBa_2Cu_4O_8$ films were grown from metal acetylacetonates [9]. In addition to organic solvents, high-molecular weight carbocylic acids can be employed as ligands for the homogeneous complexation of the required metal ions. For example, Y123 and $Bi_2Sr_2CaCu_2O_x$ (Bi2212) films and fibers were made from solutions containing poly(methylmethacrylate-co-methacrylic acid) [10] and poly(methacrylic acid) [11–13].

The use of polymer based precursors for the manufacture of films of high-T_c materials is particularly attractive, since most conventional and modern lithographic techniques use polymer layers as a medium in the pattern formation process. This was shown [14] for the photolithographic patterning of a Bi-Sr-Ca-Cu precursor film with lateral resolutions down to 20 μm. In a different approach, the high viscosity of polymer-containing precursor solutions make them amenable for a variety of soft-lithographic techniques [15].

As opposed to high-T_c films made by the more commonly used techniques, the morphology and epitaxial order of layers made by a solution deposition approach is less studied. The knowledge of the film morphology and crystalline order on sub-micrometer length scales is, however, likely to be of importance for the lithographic patterning of high-T_c thin films.

The purpose of this study is the detailed investigation of the structure and morphology of Bi2212 films made by a solution deposition process. Various X-ray diffraction techniques were employed to investigate the epitaxial order of the Bi2212 films. In addition, scanning electron microscopy (SEM) was used for complementary studies of the film morphology.

[a] *Present address:* University of Electronic Science and Technology of China, School of Microelectronics and Solid-State Electronics, Chengdu, Sichuan 610051, P.R. China.
[b] e-mail: u.steiner@chem.rug.nl

2 Experimental details

2.1 Sample preparation

Bi2212 precursor solutions were made following the procedure by von Lampe and coworkers [13]. The solvents used were 2-methoxyethanol (98%, Merck) or N,N-dimethylformamide (99%, Acros, Geel, Belgium). $Bi(NO_3)_3{\cdot}5H_2O$, $Sr(NO_3)_2$, $Ca(NO_3)_2{\cdot}4H_2O$, and $Cu(NO_3)_2{\cdot}2.5H_2O$ (98% or higher, Fluka, Aldrich) were added. Two slightly different compositions were used: 3.923:1.692:1:1.915 (sample 1) and 4.102:1.792:1:1.961 (sample 2), by weight, corresponding to the approximate molar ratio of 2:2:1:2. The solution was stirred until clear and poly(methacrylic acid) (PMAA) (Polymer Standards Service, Mainz, Germany, molecular weight $M_w = 82,400$, polydispersity $M_w/M_n = 1.03$, or comparable self-made PMAA) was added. This resulted in clear, blue-green solutions, with a composition (metal-nitrates:solvent:PMAA) of 1:2.5:1.6 by weight.

The substrates were polished $SrTiO_3$-(001) single crystals ($10 \times 10 \times 1$ mm^3, with edges parallel to [100], [010], and [001], TBL-Kelpin, Neuhausen, Germany). Before usage, the substrate surfaces were cleaned by heating to 950 °C for several hours in air.

Bi2212 precursor solutions were spin-cast onto the substrates at 4,000 rpm and dried at 80 °C for 2–3 hours. The dried films had a blue-green color and were ≈650 nm thick. They were placed in a tube-oven, through which an airflow was maintained and the temperature was varied according to the following protocol: increase from room temperature to 200 °C with 10 °C/min, from 200 °C to 500 °C with 5 °C/min, from 500 °C to 850 °C with 10 °C/min. The sample was kept at 850 °C for 1 h, and then cooled from 850 °C to ≈600 °C with 5 °C/min, followed by slow cooling to room temperature. The obtained films of 80–100 nm thickness were bright gray and transparent.

2.2 Scanning electron microscopy

The surface morphology of the annealed films was imaged with a Jeol 6320F field emission scanning electron microscope, using an acceleration voltage of 1.5 kV and a working distance of 5 mm. A typical SEM image of a ≈100 nm thick Bi2212 film is shown in Figure 1. It shows a faceted surface of terraces of 100 nm–1 μm in size.

2.3 Resistance measurements

The resistance of the films was measured in the four point mode. Platinum wires were connected to the Bi2212 films by silver paste. The sample was cooled to 50 K in a PPMS 6000 cryostat (Quantum Design, San Diego, USA). The sample resistance R was measured (Agilent multimeter 3458A) as a function of temperature T while heating at a rate of 1 K/min. Figure 2 shows $R(T)$ of two Bi2212 samples. The resistance measurements of both sample show a transition to the superconducting state in the 77–85 K temperature range, reaching 50% resistance at $T_c \approx 81$ K, in good agreement with Bi2212 films prepared by chemical vapor deposition [4]. The critical current density (see [13]) was 2×10^5 A/cm^2 and 4×10^4 A/cm^2 at 30 K for sample 1 and 2 respectively.

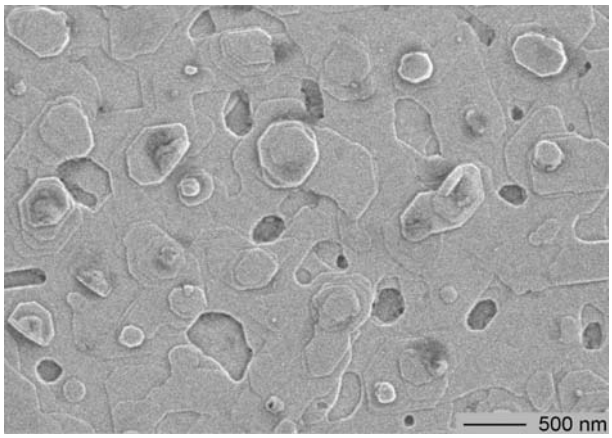

Fig. 1. SEM image of sample 2, showing a ≈100 nm thick Bi2212 film. The four directions of the steps' edges are in register with the underlying $SrTiO_3$ substrate.

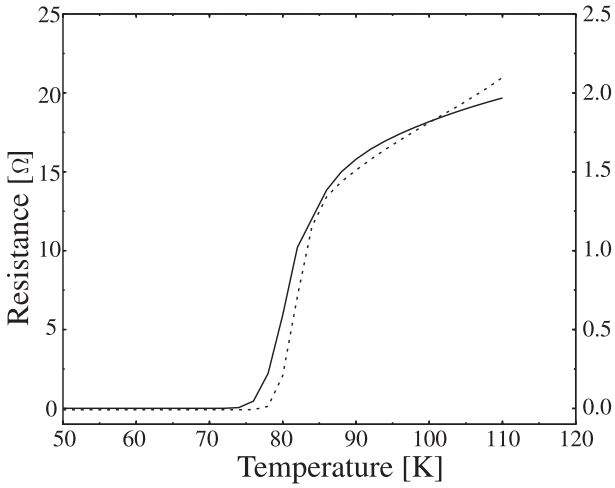

Fig. 2. Resistance of Bi2212 films as a function of temperature. The solid line corresponds to sample 1 (left axis), the dashed line to sample 2 (right axis). The critical temperatures (defined by the inflection point) are 80.8 K and 81.6 K for sample 1 and 2, respectively.

2.4 X-ray diffraction

The orientation of the crystallites with respect to the $SrTiO_3$ substrate was determined using five different X-ray diffraction experiments. To identify the different BiSrCaCuO phases with a **c**-axis orientation parallel to the $SrTiO_3$ surface normal (**c**-axis orientation), ω-2ϑ scans were taken on a Bruker Axs D8 powder diffractometer (40 kV, 40 mA, software package Diffrac Plus Basic 4.02). The quality of the **c**-axis alignment of the Bi2212 phase with respect to the $SrTiO_3$ substrate was determined by rocking curves (ω scans) taken on a Philips PW 1820 powder diffractometer (40 kV, 30 mA, software

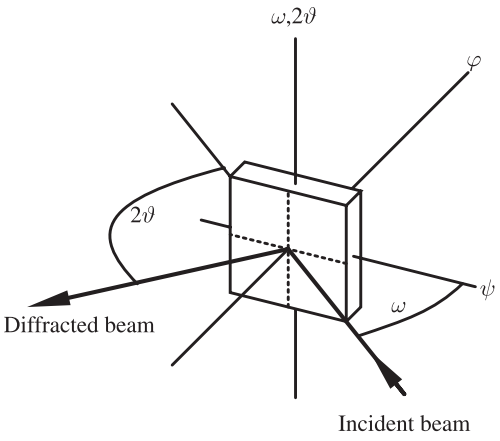

Fig. 3. The four axes of a Philips materials diffractometer, shown with $\psi = 0°$, $\varphi = 0°$.

APD PW 1877 3.6g). Texture scans ($\varphi - \psi$ scans) revealed the in-plane orientation of the Bi2212 crystallites and area scans (ω-$2\vartheta - \psi$ scans) were used to determine the in-plane orientation of the Bi2201 minority phase and to exclude the presence of other phases that had a highly symmetric lattice plane parallel to the **ac** plane of $SrTiO_3$. A second type of area scans (ω-$2\vartheta - \omega$ scans) was used to determine the averaged in-plane lattice constant $(a+b)/2$ of the Bi2212 phase. Both, texture and area scans were taken on a Philips X'Pert MRD materials diffractometer, type 3050/65 (40 kV, 40 mA, software X'Pert Data Collector 2.0b). All diffractometers were equipped with monochromators for Cu Kα_1 radiation. The notation of the scan-axes is given in Figure 3.

3 Results and discussion

Two samples were chosen for further investigation by X-ray diffraction, based on results of the SEM and resistance measurements. Figures 4 and 5 show ω-2ϑ scans taken of both samples. Both figures show the $(00l)$ reflections of $SrTiO_3$ and a set of $(00l)$ peaks that can be assigned to the Bi2212 phase with the **c**-axis oriented parallel to the substrate normal. The differing intensities are due to different scanning conditions in terms of counting time per angle increment.

Figure 4 shows some additional peaks of lower intensities, indicative for the $(00l)$ reflections of the $Bi_2Sr_2CuO_x$ (Bi2201) phase. We attribute the presence of a Bi2201 phase in sample 1 to the somewhat different Bi:Sr:Ca:Cu composition of the precursor compared to sample 2. The presence of a small amount of Bi2201 in the Bi2212 matrix has, however, only a marginal influence on T_c (see Fig. 2).

The quantitative analysis of the $(00l)$ reflections yields the c-lattice constants of the two phases. For the Bi2212 phase, we find values of 30.70(6) Å and 30.76(1) Å for sample 1 and 2, respectively. The Bi2201 phase in Figure 4 had a c-lattice constant of 24.40(1) Å.

The mosaic spreads of the $SrTiO_3$-(002) and Bi2212-(006) peak were further analyzed by ω scans

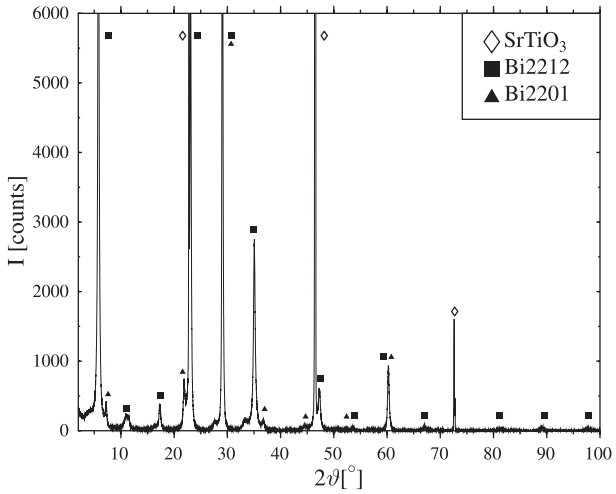

Fig. 4. ω-2ϑ scan of sample 1. Apart from the $SrTiO_3$ and Bi2212 signal, several additional peaks are discernible. Some of these peaks can be attributed to a $Bi_2Sr_2CuO_x$ (Bi2201) minority phase. The unassigned peaks indicate the presence of at least one further (unidentified) phase.

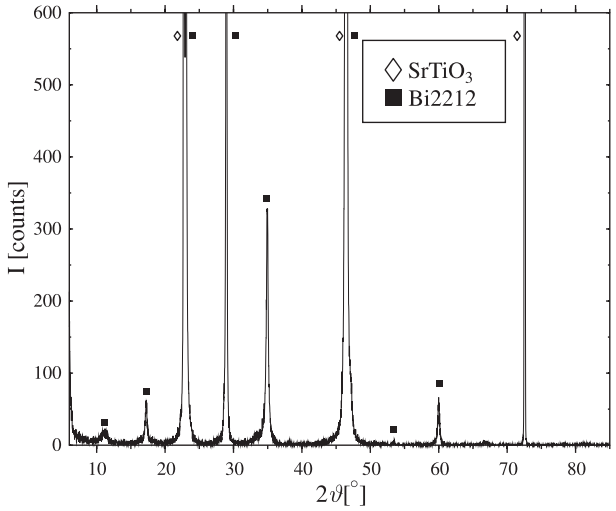

Fig. 5. ω-2ϑ scan of sample 2. As opposed to Figure 4, only reflections from the $SrTiO_3$ substrate and Bi2212 film are visible, indicating a better purity of the superconducting film.

(so-called rocking curves). The full-width-half-maximum (FWHM) of the $SrTiO_3$-(002) peak was 0.83° and 0.85° for sample 1 and 2, respectively. The Bi2212-(006) reflections had an angular spread of 0.89° for sample 2, as shown in Figure 6 and 1.1° for sample 1. This indicates that the mosaic spread of the film is slightly higher than that of the substrate, in contrast to previous reports of equal mosaic spreads of substrate and film (with FWHMs of 0.25°) [16].

3.1 In-plane orientation

To establish the in-plane orientation of the Bi2212 phase, textures scans ($\varphi - \psi$ scans) were performed. The substrates were aligned on a four-axis goniometer using the $SrTiO_3$-(002) and -(101) reflections so that at $\varphi = 0°$

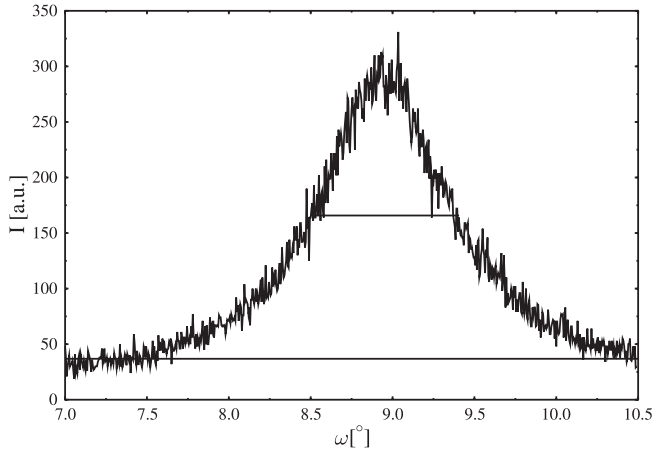

Fig. 6. Rocking curve (ω scan) of the Bi2212-(006) peak of sample 2 at $2\vartheta = 17.56°$. The FWHM with of 0.89° is a measure for the accuracy of the **c**-axis alignment of the epitaxial Bi2212 phase.

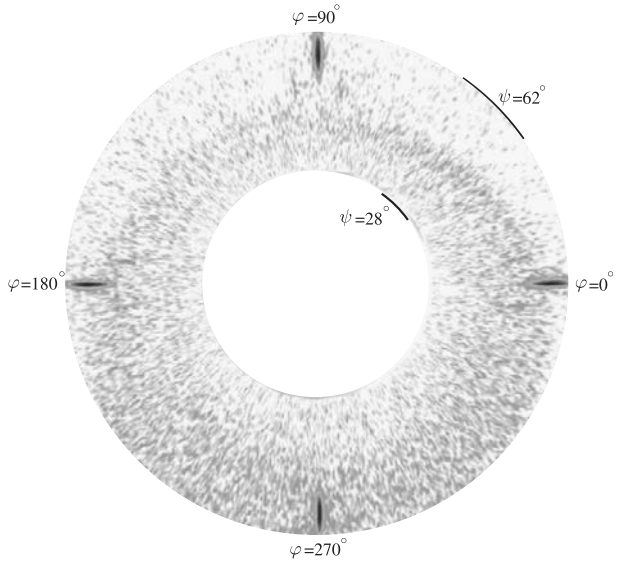

Fig. 7. Texture scan ($\varphi-\psi$ scan) of the Bi2212-{115} reflection of sample 1. The four peaks at $\varphi = 0°, 90°, 180°$, and 270°, are characteristic for a **c**-axis aligned Bi2212 phase with an in-plane orientation of **a** parallel to the $SrTiO_3$-[110] or -[$\bar{1}$10] direction. The elongated peak shape is a consequence of the X-ray beam profile ($1 \times 10\,\mathrm{mm}^2$ line focus).

the $SrTiO_3$-[100] direction was in the plane of diffraction. Since the Bi2212-{115} reflections do not overlap with any of the $SrTiO_3$ peaks they were chosen to investigate the orientation of the **a**- and **b**-axes, with lattice constants [17] of $a = 5.410(3)$ Å, $b = 5.439(5)$ Å. The Bi2212-{115} texture scan of sample 1 is shown in Figure 7. The (115) direction forms an angle of approx. 58.06° with the **c**-axis. Therefore, for **c**-axis oriented material the {115} reflections appear at $\psi = 58.06°$. Assuming a 'cube on cube'-type growth of Bi2212, where the **a**-axis of Bi2212 is parallel to the [110] or [$\bar{1}$10] substrate directions, the Bi2212-{115} reflections should appear at $\varphi = 0°, 90°, 180°, 270°$. This is borne out by the

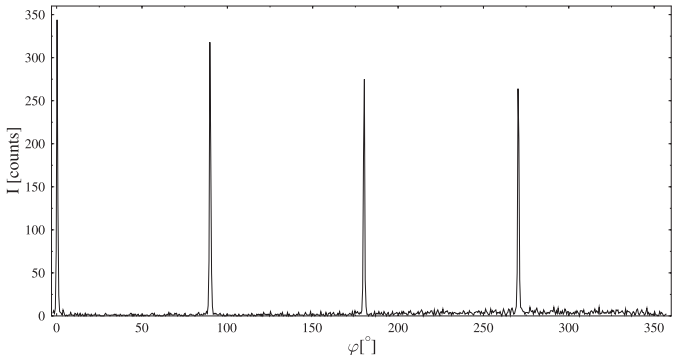

Fig. 8. φ scan extracted from Figure 7 for $\psi = 58°$. The width of the four peaks is 1.1°.

data in Figure 7, showing four strong peaks at the predicted positions. In Figure 8, a single φ scan was extracted from Figure 7 for $\psi = 58°$, showing the peak positions in more detail. The four peaks are centered at $\varphi = 0.2°, 89.8°, 180.2°, 270.4°$ and have a FWHM of 1.1°. The angular spread is comparable to that found for Y123 films [5] of approx. 1.5°, but higher than observed in Bi2212 films by others [1].

Since the *c*-lattice constant of Bi2212 is $\approx 8 a_{SrTiO_3}$, it may be possible for Bi2212 to grow epitaxially with its **c**-axis parallel to the [100] or [010] direction of $SrTiO_3$. Therefore, an epitaxial Bi2212 phase with the **c** and either the **a** or the **b**-axes oriented parallel to the substrate surface seems possible. Epitaxially even more favorable is material where the **a** + **b** and **c** directions are parallel to the $SrTiO_3$ surface, since $a_{Bi2212}\sqrt{2} \simeq 2a_{SrTiO_3}$. The {115} reflections of this first epitaxial orientation should appear in Figure 7 at $\psi = 90° - 58.06° = 31.94°$ (and $\varphi = 0°, 90°, 180°, 270°$). **a** + **b**-axis oriented material corresponds to peak positions at $\psi = 53.13°$ (and $\varphi = 0° \pm 48.60°, 90° \pm 48.60°$, etc.). Not only are none of these predicted peaks visible in Figure 7, the absence of any discernible peaks (or ring-pattern) other than the four peaks that are attributable to the **c**-axis oriented Bi2212 phase indicates the absence of detectable amounts of Bi2212 with a different epitaxial orientation.

Sample 1 was further studied to investigate the presence of the Bi2201 material or other phases. Bi2201 ($a = 5.37$ Å, $b = 5.37$ Å[18]) has a much lower critical temperature (T_c between 6 K and 10 K) [19,20] or may not be superconducting at all [18,21]. Since the metal-composition of sample 1 was somewhat off-stoichiometric, other phases may have grown epitaxially. Area-scans (ω-$2\vartheta - \psi$ scans) of the $\mathbf{a}^*\mathbf{c}^*$ plane of $SrTiO_3$ can reveal the presence of suitably oriented minority phases. Figure 9 shows two columns of peaks that can be attributed the $SrTiO_3$ substrate and **c**-axis oriented Bi2212 and Bi2201 phases. This reciprocal lattice plane was chosen because it contains the ($h0l$) reflections of $SrTiO_3$ and the (hhl) reflections of **c**-axis oriented Bi2212 and Bi2201 with an in-plane orientation where $\mathbf{a}_{Bi2212}$ and $\mathbf{a}_{Bi2201}$ lie parallel to the $SrTiO_3$-[110] and -[$\bar{1}$10] directions. The appearance of these peaks in Figure 9 not only confirms the results for sample 2 (Fig. 7)

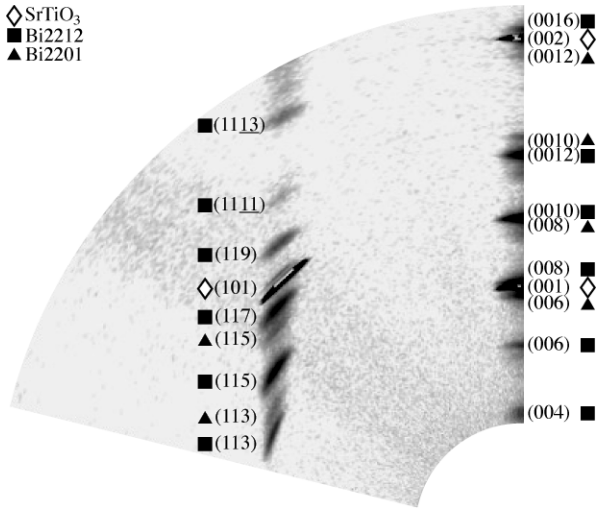

Fig. 9. Area scan (ω-$2\vartheta - \psi$ scan) of the $\mathbf{a}^*\mathbf{c}^*$ plane of $SrTiO_3$ (sample 1). The peaks (logarithmic grayscale) are indicative of **c**-axis oriented Bi2212 and Bi2201 phases with an **a**-axis orientation parallel to the [110] or [$\bar{1}$10] substrate direction.

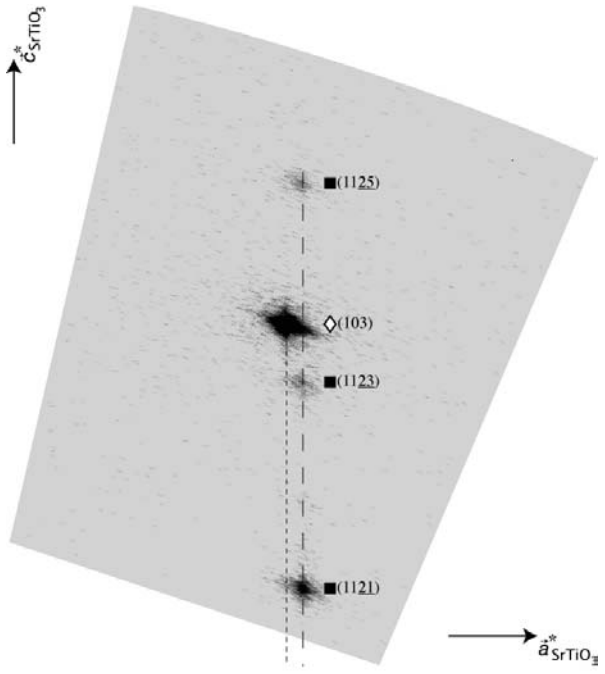

Fig. 10. Area scan (ω-$2\vartheta - \omega$ scan) of the $\mathbf{a}^*\mathbf{c}^*$ plane of $SrTiO_3$ (sample 1). The dominant peak is the (103) substrate peak. The horizontal shift of the three Bi2212 peaks (dashed line) with respect to the $SrTiO_3$ peak (dotted line) can be used to calculate the averaged in-plane Bi2212 lattice constant $(a+b)/2$.

for the Bi2212 phase, but also shows that the Bi2201 minority phase has the same in-plane orientation as Bi2212.

To determine the averaged in-plane lattice constant $(a+b)/2$ of the Bi2212 phase a second type of area scan was performed (Fig. 10). Instead of the stepwise rotation of the sample around the ψ-axis as in Figure 9, the offset in ω was stepwise varied. The advantage of this scan type

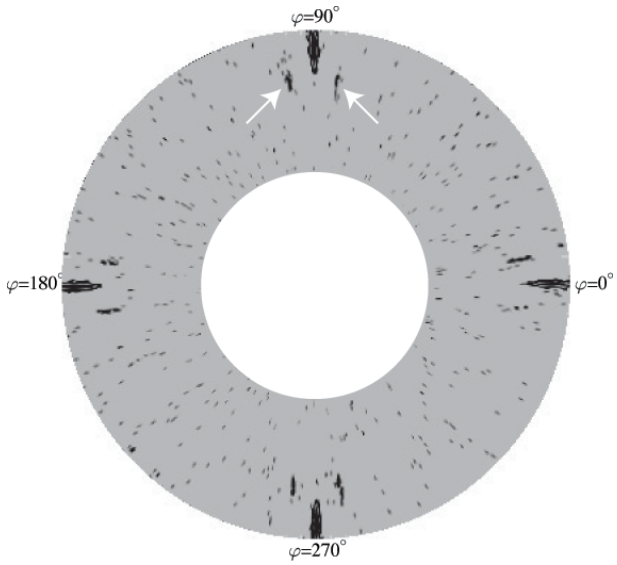

Fig. 11. Texture scan of of an additional sample. In the $\mathbf{a}^*\mathbf{c}^*$ plane of Bi2212, each primary reflection is accompanied by two satellite peaks. These peaks (a subset of 8 satellite peaks per main reflection) are indicative of a superstructure along the *b*-axis of Bi2212 with a periodicity of 5 unit cells [17].

is the symmetrical appearance of the peaks, despite the elongated beam profile (line focus) used in the diffraction experiment. Figure 10 shows the reciprocal space around the (103) reflection of $SrTiO_3$. Three peaks of the Bi2212 phase can be discerned, lying on a vertical line (dashed line in Fig. 10) in the $\mathbf{a}^*\mathbf{c}^*$ plane. The horizontal position of the Bi2212 reflections with respect to the substrate peak (dotted line) can be used to determine the in-plane lattice constant of the Bi2212 unit cell. Since the **a**-axis of epitaxial Bi2212 coincides with the $\mathbf{a}+\mathbf{b}$ diagonal of the substrate lattice (i.e. the Bi2212 **ab** plane is rotated by 45° around **c** with respect to the $SrTiO_3$ lattice), the location of the Bi2212 peaks yields the averaged in-plane lattice constant. Compared to $a = 3.905\,\text{Å}$ for $SrTiO_3$ we find for Bi2212 $(a+b)/2 = 5.422\,\text{Å}$ for sample 1 and $(a+b)/2 = 5.438\,\text{Å}$ for sample 2, in good agreement with the bulk value of 5.425 Å. This measurement reveals a lattice mismatch of 1.8% and 1.5% (for sample 1 and 2, respectively) of the Bi2212 with respect to $SrTiO_3$.

3.2 Superstructure

The texture scans of the Bi2212-{115} reflections of both samples show a pair of weaker peaks that lie symmetrically on both sides ($\pm\Delta\varphi$) of each {115} peak at higher ψ values. These additional peaks are better visible in a Bi2212-{115} texture scan of a third, identically prepared sample (Fig. 11). The four {115} peaks are clearly surrounded by pairs of satellite peaks at $\psi \approx 49.5°$ (indicated by arrows in Fig. 11). Their positions in φ are approximately ±6.5° around the 0°, 90°, 180°, and 180° primary reflections. An area scan (not shown) of the $SrTiO_3$ [110] $\mathbf{c}^*$ plane of a further superconducting

sample (containing the Bi2212-($h0l$) reflections) shows similar weak peaks that lie on both sides of the extinguished ($00l$) and ($20l$) reflections (for odd values of l). The lateral distance of satellites of equal l is approximately the same compared to neighboring visible ($00l$) main peaks (even values of l), i.e. close to $2c^*$, indicative of a periodicity of ~ 30 Å in the Bi2212-**a** and -**b** direction. This is in accordance with the well known incommensurate modulation of the metal ion positions along the **b**-axis, leading to a superstructure with a periodicity of $4.5b - 5b$ [22,23].

Due to the fourfold rotational symmetry of $SrTiO_3$ substrate, **c**-axis oriented Bi2212 domains exhibit two in-plane orientations with **a** parallel to $SrTiO_3$-[110] and -[$\bar{1}$10]. The observation of the satellites in both the $SrTiO_3$ [110] $\mathbf{c}^*$ area scan and the Bi2212-{115} texture scan indicates that each visible Bi2212 peak is surrounded by eight satellite reflections forming a tetragonal prism, the center of which is being occupied by the Bi2212 main peak. The height of the prism is $2c^* \approx 2/30.7$ Å the width of the prism is $2b^*/4.5 - 2b^*/5$. Our thin film results therefore reproduce the measurements of single crystals.

3.3 Crystal morphology

The in-plane orientation of the Bi2212 phase as determined by X-ray diffraction could also be verified by the morphology of the epitaxial crystallites. In Figure 1 four distinct directions of the crystal edges can be identified. These edges form mutual angles of 45° and 90°. By reducing the SEM magnification, the entire sample becomes visible. This way, it was verified that two of these four directions are parallel to the edges of the substrate, that is, the [110] and [$\bar{1}$10] edges of Bi2212 are parallel to the [100] and the [010] directions of $SrTiO_3$, respectively. Since the Bi2212-(001) crystal face forms terraces that are parallel to the substrate surface, the crystallite edges correspond to the (100), (010), (110), and ($\bar{1}$10) faces, which are perpendicular to the $SrTiO_3$ surface.

4 Conclusion

In summary, we have investigated the epitaxial order of $Bi_2Sr_2CaCu_2O_x$ films that were solution deposited onto a $SrTiO_3$-(001) substrate. The films consisted mainly of the superconducting Bi2212, with a **c**-axis orientation perpendicular to the substrate surface and an in-plane (**a**-axis) orientation parallel to the [110] or [$\bar{1}$10] direction of $SrTiO_3$. The formation of the epitaxial Bi2212 from the polymer metal precursor is reasonably robust. When deviating from the stoichiometric ratio of metal ions required to form the Bi2212 phase, a minority epitaxial Bi2201 phase and a small amount of an unidentified phase were observed (see Fig. 4). The presence of these additional phases has no significant influence on the epitaxial growth of the majority Bi2212 phase, nor on the transition temperature to superconductivity.

The relative ease of the manufacture of solution deposited layers, combined with a certain robustness in composition makes this system a promising candidate for employing soft-lithography [15] to manufacture superconducting thin films with lateral structures on the micrometer scale.

The authors thank U. Wiesner, R. Ullrich and S. Walheim for their important role in the initial phase of this project, T.T.M. Palstra for access to his cryostat, F. Zygalsky for the critical current density measurements, and J. Baas for his help with the resistance measurements. The SEM images were taken by H. Nijland and some of the PMAA was synthesized by W. Belgraver. Partial financial support was provided by the Dutch "Stichting voor Fundamenteel Onderzoek der Materie" (FOM).

References

1. C. Maréchal, E. Lacaze, W. Seiler, J. Perrière, Phys. C **294**, 23 (1998)
2. R. Kromann, J.B. Bilde-Sørensen, R. de Reus, N.H. Andersen, P. Vase, T. Freltoft, J. Appl. Phys. **71**, 3419 (1992)
3. D. Dimos, P. Chaudhari, J. Mannhart, Phys. Rev. B **41**, 4038 (1990)
4. J. Stejskal, J. Leitner, D. Sedmidubský, M. Nevřiva, P. Beran, A. Strejc, J. Cryst. Growth **210**, 587 (2000)
5. A. Ignatiev, P.C. Chou, Y. Chen, X. Zhang, Z. Tang, Phys. C **341-348**, 2309 (2000)
6. S.R. Breeze, S. Wang, J. Mat. Sci. **34**, 1099 (1999)
7. C.E. Rice, R.B. van Dover, G.J. Fisanick, Appl. Phys. Lett. **51**, 1842 (1987)
8. L.F. Admaiai, P. Grange, B. Delmon, M. Cassart, J.P. Issi, J. Mat. Sci. **29**, 5817 (1994)
9. T. Manabe, Y. Yajima, I. Yamaguchi, T. Kumagi, T. Shimizu, S. Mizuta, Phys. C **303**, 53 (1998)
10. J.C.W. Chien, Polym. Bull. **21**, 1 (1989)
11. J.C.W. Chien, B.M. Gong, J.M. Madsen, R.B. Hallock, Phys. Rev. B **38**, 11853 (1988)
12. I. von Lampe, F. Zygalsky, G. Hinrichsen, H. Springer, H. Schubert, J. Mat. Sci. Lett. **21**, 133 (2002)
13. I. von Lampe, A. Schmalstieg, S. Götze, J.-P. Müller, F. Zygalsky, H.-J. Lorkowski, M. Matalla, J. Mat. Sci. Lett. **16**, 16 (1997)
14. I. von Lampe, private communication
15. Y. Xia, J.A. Rogers, K.E. Paul, G.M. Whitesides, Chem. Rev. **99**, 1823 (1999)
16. G. Balestrino, M. Marinelli, E. Milani, A. Paoletti, P. Paroli, J. Appl. Phys. **68**, 361 (1990)
17. R.M. Hazen et al., Phys. Rev. Lett. **60**, 1174 (1988)
18. Y. Mei, S.M. Green, C. Jiang, H.L. Luo, J. Appl. Phys. **64**, 6795 (1988)
19. J.B. Torrance, Y. Tokura, S.J. LaPlaca, T.C. Huang, R.J. Savoy, A.I. Nazzal, Solid State Comm. **66**, 703 (1988)
20. J.M. Tarascon, W.R. McKinnon, P. Barboux, D.M. Hwang, B.G. Bagley, L.H. Greene, G.W. Hull, Y. LePage, N. Stoffel, M. Giroud, Phys. Rev. B **38**, 8885 (1988)
21. X. Zhu, G.C. Xiong, R. Liu, Y.J. Li, G.J. Lian, Z.Z. Gan, Physica C **216**, 153 (1993)
22. X.B. Kan, S.C. Moss, Acta Cryst. B **48**, 122 (1992)
23. L. Shan, A. Ejov, A. Volodin, V.V. Moshkalov, H.H. Wen, C.T. Lin, Europhys. Lett. **6**, 681 (2003)